ADVANCED INTELLIGENT SYSTEMS
Open Access
www.advintellsyst.com

Self-Regulated Self-Healing Robotic Gripper for Resilient and Adaptive Grasping

Huijiang Wang, Seppe Terryn, Zhanwei Wang, Guy Van Assche, Fumiya Iida, and Bram Vanderborght*

Flexible, soft materials are increasingly used for the fabrication of soft robots, as the inherent compliance and shock-absorbance protect the robot from mechanical impact. Soft universal grippers take full advantage of this adaptability, facilitating effective and safe grasping of various objects. However, due to their predominantly soft material composition, these grippers have limited lifetimes, especially when operating in unstructured and unfamiliar environments. The self-healing universal gripper (SHUG) is proposed, which can grasp various objects and recover from substantial realistic damages autonomously. It integrates damage detection, heat-assisted healing, and healing evaluation. Notably, unlike other universal grippers, the entire SHUG can be fully reprocessed and recycled. The gripper's functionality relies on the particle jamming of steel balls enclosed within a self-healing membrane. Thanks to the thermoreversible covalent Diels–Alder bonds in self-healing polymer membrane, the gripper is able to recover from macroscopic damages including scratches and punctures. Temperature-assisted healing is regulated in a closed-loop manner using an embedded thermocouple and Joule heater. Experimental validation demonstrates the adaptability, resilience, and recyclability of the SHUG.

1. Introduction

Universal robotic grippers are renowned for the ability to grasp arbitrarily shaped objects and adapt to any shapes without sensory feedback.[1,2] These universal grippers, which are typically made out of granular particles encapsulated by a deformable latex rubber membrane, can flow around and conform to the shape of a target object, when pressed against it.[3–5] With vacuum pressure control, the gripper can achieve a morphological transition from an unjammed, flexible state to a jammed state with solid-like rigidity, allowing them to reliably grip and hold objects with masses that are even several times their weight. Although, granular jamming is the most common stiffness modulation technology in universal grippers, also origami-based[6] and shape memory polymer (SMP)-driven systems exist.[7] In contrast to conventional multifingered designs with many dependently actuated joints that require a complex computational decision-making algorithm to control the amount of stress and where to apply, universal grippers perform robotic manipulations for multiple objects with an all-in-one solution and reduced hardware and software complexity.[8,9] This functionality that relies on the interaction of the system and its environment rather than on complex control is a perfect example of embodied intelligence.[10,11]

Traditional universal soft grippers are mostly made out of flexible elastomeric polymers including silicones,[12–14] polyurethanes,[15–17] and SMPs[7] with modulus of 10^5–10^6 Pa. This is comparable to biological compliance of organisms (moduli of 10^3–10^7 Pa), making these materials promising for safe human–machine interaction (HMI).[18–20] Featuring inherent compliance, soft and flexible materials serve as shock-absorbing media that create energy-storing behaviors against abrupt and sudden mechanical impact.[6,21–23] This allows a universal gripper to conform to, grasp, and handle objects with varying shapes in uncertain, dynamic task environments.[3,24,25] The universal soft gripper, however, comes at a cost, as the vulnerability of the soft membrane limits their lifetime (50 000 grips), in particular in the presence of sharp objects (5000 grips).[1] Sharp objects or rough surfaces perforate the soft cover, leading to a loss of air tightness in the gripper, which is fatal for the soft gripper that loses its functionality. Even in the absence of sharp

H. Wang, F. Iida
Bio-Inspired Robotics Lab
Department of Engineering
University of Cambridge
Trumpington Street, Cambridge CB2 1PZ, UK
E-mail: hw567@cam.ac.uk

S. Terryn, Z. Wang, B. Vanderborght
Brubotics
Vrije Universiteit Brussel and Imec
Pleinlaan 2, 1050 Elsene, Belgium

S. Terryn, G. Van Assche
Physical Chemistry and Polymer Science (FYSC)
Vrije Universiteit Brussel
Pleinlaan 2, 1050 Elsene, Belgium

The ORCID identification number(s) for the author(s) of this article can be found under https://doi.org/10.1002/aisy.202300223.

DOI: 10.1002/aisy.202300223

objects, other damaging conditions, including fatigue, overload, and interfacial debonding, over time also lead to leaking.[26] In most cases the polymer cover is not reprocessable, and as such a damaged gripper cannot be recycled. Because of this poor recyclability and limited lifetime, the large adoption of universal grippers is prevented as they are seldom competitive with alternative gripping technologies on an economic or sustainability level.

One promising remedy to the high vulnerability is to construct the gripper from self-healing (SH) polymers.[12,26–28] Having the capacity to heal, the self-healing elastomeric membrane of the universal gripper can remain soft, required for its gripping functionality, yet can recover from macroscopic damages, extending its lifetime. Through the addition of fillers or ionic liquids, self-healing elastomers or gels can be made electronic conductive, making them promising for self-healing flexible electronics,[29,30] including strain sensors.[31–33] SH elastomeric polymers are classified into two types, based on the spontaneity of the healing process. The first category is composed of autonomous SH polymers, in which healing occurs at ambient temperature without the aid of any external stimulus (e.g., heat or light). Most common healing mechanisms rely on hydrogen bonds,[34–38] π–π cross links,[39,40] or metal–ligand complexes.[41,42] However, achieving rapid healing at ambient temperature in combination with high mechanical performance and stability is a challenge yet to be solved by the self-healing materials community.[26,43] However, high mechanical strength and Young's modulus and creep resistance are needed to create soft robots and grippers that have acceptable payloads. Consequently, nonautonomous SH polymers, in which healing relies on stronger reversible chemistries and has superior mechanical properties, are more suitable for these robotics applications. Their healing is activated by an external trigger, which can be heat or light. Most common examples are based on thermoreversible covalent bonds, like dissociative chemistry (e.g., Diels–Alder [DA])[44,45] or associative chemistry (e.g., thiol–disulfide)[46] or on photoreversible properties.[47] Damage can only be healed in a reasonable time frame (e.g., hours) by heating the material (typically to 50–90 °C) or exposing to UV light irradiation (a combination of UV and visible light), increasing both the reactivity and mobility in the polymer network. Although multiple self-healing actuators have been proposed and integrated into robotic systems, ranging from multifingered grippers[46,48] to artificial muscles,[44,49] the healing has mostly been controlled by bulky external systems, including ovens or UV lamps, rather than from integrated systems.

In this research, we proposed a particle jamming-based universal gripper with the intrinsic self-healing ability to recover from macroscopic damages that result from functioning in an unstructured and dynamic environment. This self-healing universal gripper (SHUG) combines universal adaptation, resulting from granular jamming of steel balls encapsulated in a flexible membrane, with resilience to damage due to autonomous healing via an embedded heating system (e.g., an integrated heat cartridge) and self-healing polymers (**Figure 1**). The outer flexible membrane, which is the most vulnerable component and that is in direct contact with the environment during gripping, was constructed of a self-healing elastomer. We exploit reversible covalent polymer networks that were developed and characterized with temperature-based equilibrium shift,[45] in which healing relies on the thermally triggered DA chemistry. However, special efforts were made in this article to develop a new

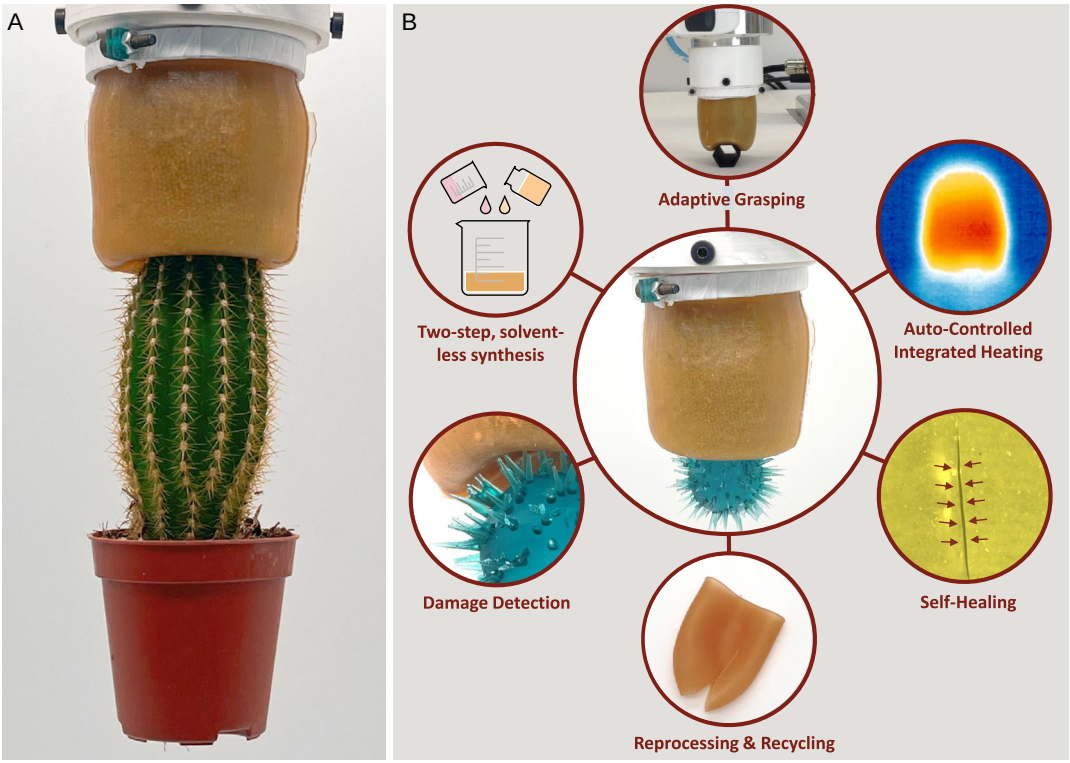

Figure 1. A) SHUG is adaptively grasping a hazardous object (cactus) and B) the highlights of the integrated system.

synthesis that is more sustainable, excluding the need of chloroform, a carcinogenic solvent.

The placement of the heater and the morphology of the gripper are rigorously designed using a thermal conductivity model to maximize the heat transfer through the particle to the outer layer of the gripper (e.g., the self-healing membrane). Excellent heat distribution is achieved via judicious choice of the in-filled particles (e.g., steel balls) to enlarge heat conductivity. In addition, design parameters, including the membrane thickness, mechanical properties of the self-healing polymers, and geometric design, have been optimized to achieve high-quality adaptive grasping. These design parameters were tuned using a finite-element analysis (FEA)-based morphological optimization prior to the practical fabrication and experimentation on the SHUG, which was placed as end effector on a robotic manipulator.

Grasping performance is validated by measuring the maximum holding force (MHF) on objects with varying shapes and sizes. The self-healing ability was demonstrated via healing of a series of damages, ranging from local small damage including scratch and puncture to fatal damage such as cut and tear, first on a material level through tensile testing and later on the gripper level. The healing in the SHUG is carried out autonomously via a closed-loop temperature control using the integrated heater and a thermocouple. Finally, in high contrast to conventional elastomers, the proposed DA elastomers can be reprocessed through heat treatment. Consequently, we demonstrate that upon catastrophic damages, too large to heal, the entire SHUG can be completely reprocessed and reshaped into a new gripper using casting at high temperatures (see Video S1, Supporting Information). Aside from healing, this high recycling potential can further increase the sustainability of universal grippers and soft robotics in general in the future.

2. Results

2.1. Principle of the SHUG

The universal adaptive gripper's design concept is based on particle jamming.[1] The universal gripper consists of two essential components: the flexible and deformable cover and the particles which fill the cavity in the cover (**Figure 2**D). Because the flexible cover is the only interface in direct contact with the environment, it is the most vulnerable part in the presence of sharp objects or surfaces. To address this challenge the cover will be produced out of a self-healing polymer. To manipulate a range of objects, the jamming gripper was attached to a robotic manipulator, a Franka Emika. A host computer (Host PC) is utilized to implement the upstream sensory feedback and downstream control over the entire system including the robot manipulator, the pneumatic switch on/off of the gripper, and the embedded heating element. The integrity of the gripper's airtightness can be compromised when it is subjected to external hazards, resulting in damage. To detect such damage, a pressure sensor is employed to monitor any pressure drop caused by a perforation. Upon detecting damage, the Host PC sends commands to the robot arm, instructing it to go to a specific orientation (upside down) that maximizes contact between the metal balls and the heater. This also helps to prevent (further) particle leakage from the soft membrane and offers fundamental alignment of the fractured interfaces. Subsequently, the heating element is activated to increase the gripper's temperature to the desired level where the healing takes place, followed by a controlled heat–cool cycle. It is important to note that this entire workflow, encompassing damage detection, reorientation, and temperature regulation, is performed autonomously without any external human intervention. After this autonomous healing procedure, the system is as good as new and can regain its tasks.

2.2. Design and Simulation of the SHUG

As described in a review paper,[26] DA-based self-healing polymers combine an excellent healing capacity with mechanical strength and stability. Therefore DPBM-FT3000-r0.5, a self-healing polymer based on the DA reaction, is used in this paper. This polymer has excellent mechanical stability and strength and can heal at moderated temperatures and it is cast into the membrane shape during the last stage of the synthesis procedure (see Supporting Information). A cover that is too stiff will lead to inadequate adaptation to the object, whereas a cover that is too soft will lack the ability to retain shape stability. Therefore DPBM-FT3000-r0.5 is selected as it has Young's modulus of 0.57 MPa, measured via linear regression in the 0.5% strain window in a tensile test with a strain rate of $1\%\,s^{-1}$ until fracture (Figure 8B).

The geometry of the cover consists of a cylinder with a length of 60 mm and a diameter of 50 mm and a semisphere with a diameter of 50 mm. This cover is filled with particles and pinched between a base and a collar into a 3D-printed polylactic acid (PLA) holder, which is connected to the Franka manipulator and the vacuum controller (Figure 2A,B). The self-healing of the membrane is dependent on the equilibrium shift of the DA reaction, which requires a delicately controlled temperature treatment. To achieve this, first we embedded a heating element, a cartridge (40 mm, 50 W, 220 V ac), into the center of the gripper, such that the heat can be transferred homogeneously to the outer self-healing cover (Figure 2E). The cartridge heater will first heat the surrounding particles before transferring the heat to the membrane. To have a closed-loop control of the cover temperature, a thermocouple (RS PRO, Type K) was utilized as the feedback sensor. To account for heat loss during omnidirectional heat transfer, we used thermal conduction and convectional cooling model.

The design of SHUG is optimized based on the selection of the particle type and the thickness of the self-healing cover. Based on a trade-off between density, fluidity, and thermal conductivity, a number of possible particles are examined for the gripper interface such that it is able to achieve morphological self-stabilization without much internal friction between particles while also allowing heat generated at the central median to be transferred to the SH membrane with equal gradient distribution. Prior to building the physical prototype, we utilized finite element analysis (FEA) to optimize the geometric parameters of the self-healing cover in order to achieve an appropriate membrane thickness and body morphology. The particle selection and FEA simulation are substantiated in the Experimental Section.

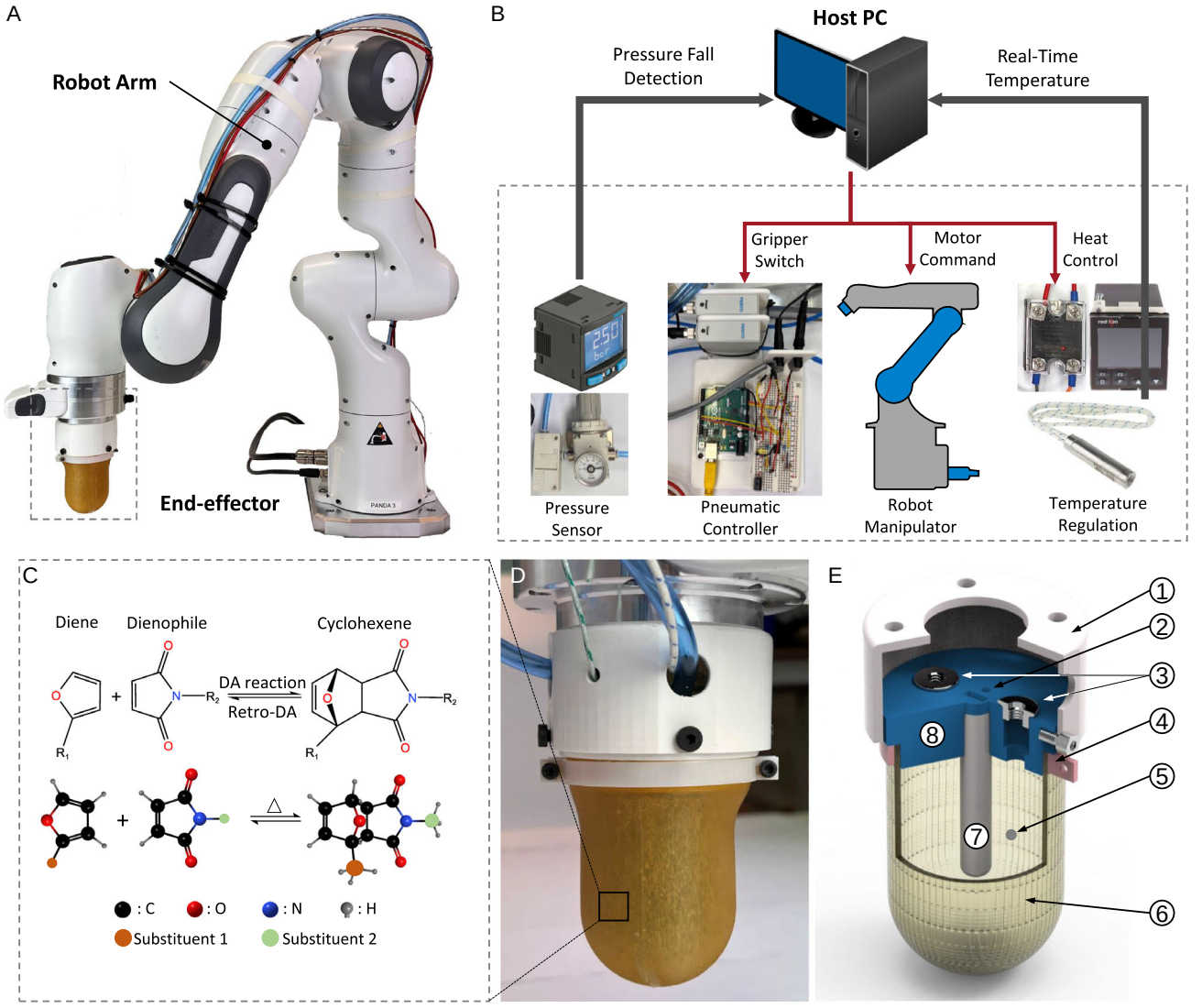

Figure 2. Design and integration of the grasping system. A) The prototype consists of a Franka robot manipulator and the fabricated SHUG as the end-effector. B) Workflow of the integrated system, where the host computer (Host PC) controls the manipulator's orientation, pneumatic regulation of the SHUG for grasping, and triggers the heating element for self-healing upon damage detection. The system utilizes a pressure sensor to inspect the airtightness and ensures real-time temperature monitoring for closed-loop heat regulation. C) The design of the self-healing interface exploits an equilibrium reaction between a diene and a dienophile that forms cyclohexene. D) Image of the fabricated SHUG and E) the corresponding assembly drawing of the SHUG including components: 1) base, 2) thermocouple mounting hole, 3) vacuum outlet ports, 4) mounting collar, 5) metal balls, 6) DA membrane, 7) embedded heating cartridge, 8) holder. The DA polymer is pinched between the holder and collar to produce an airtight seal.

2.2.1. Particles Selection

Traditional universal grippers commonly use coffee powder as an in-filling material. However, the poor flowability of coffee powder poses challenges for the gripper in terms of unjamming and resetting. Although a positive pressure control approach has been utilized to partially address this issue,[8] it introduces the need for an additional pressure source, adding complexity to the system. In our study, we considered various materials, including salt, sand, and polymers, taking into account their density, granular fluidity, and particularly, thermal conductivity (as shown in **Table 1**). Thermal conductivity plays a crucial role in facilitating heat transfer from the embedded heater to the outer region of the gripper, thereby enabling heat-stimulated healing in the membrane. Fluidity is essential for the universal gripper as it promotes better adaptation to objects, increasing the contact surface during gripping. Additionally, it facilitates object release through gravity-based self-unjamming upon pressure increase. Steel balls were selected for the design of the SHUG due to their favorable combination of excellent thermal conductivity and fluidity, attributed to minimal friction between the particles. However, it is worth noting that one drawback of using steel balls is their high density (as indicated in Table 1), resulting in an increase in the gripper's weight (e.g., 493.87 g in this design compared to the coffee powder media).

Table 1. Potential candidates for particle jamming.

	Density [g cm^{-3}]	Thermal Conductivity [W (m K)$^{-1}$]	Three-level Grading of Fluidity in the form of Granules (G) or Balls (B)
Coffee powder[55]	0.91	0.099	Low (G)
Crystalline salt[56]	2.16	0.12	Middle (G)
Dry sand[57]	1.60	0.25	Middle (G)
Polymeric[58]	0.93–0.97	0.1–0.5	Middle (G), High (B)
Silica ceramics[59]	2.60	1.50	Low (G), High (B)
Steel[60]	8.00	50.2	Low (G), High (B)

2.2.2. FEA-Based Morphological Design

The optimal thickness of the self-healing polymeric cover was determined through FEA simulations conducted in Abaqus. These simulations aimed to investigate the influence of different cover thicknesses on the gripping performance of the robotic gripper when interacting with a rigid object, specifically a sphere with a diameter of 25 mm. Our focus was primarily on assessing how the cover thickness affects two crucial parameters: the contact area between the cover and the object and the stress distribution within the flexible cover (refer to **Figure 3**A). By analyzing the results, we observed that a larger contact area between the cover and the object leads to a more secure interlocking mechanism, while a lower stress distribution within the cover makes the object less likely to be crushed, bruised, or damaged. As the soft cover comes into contact with the rigid sphere, it undergoes deformation, with localized high pressure concentrated at the point of initial contact (as indicated by the Von Mises Stress in Figure 3B). Figure 3C demonstrates the relationship between the cover thickness and the two significant gripping parameters: contact area and stress. Notably, we observed that a cover thickness of 2 mm achieved the largest contact area while maintaining minimal stress levels. Furthermore, in addition to optimizing the membrane thickness, we also compared the material with varying levels of Young's modulus, ranging from 0.2 to 1 MPa. After careful evaluation, we selected Young's modulus of 0.57 MPa as the most suitable for our design. An overview of the final design parameters is illustrated in **Table 2**.

2.2.3. Thermodynamic Model of Heat Transfer

Upon damage in the SHUG, the self-healing program is launched, which consists of heating the self-healing cover. However, precise temperature control is critical as: 1) too low

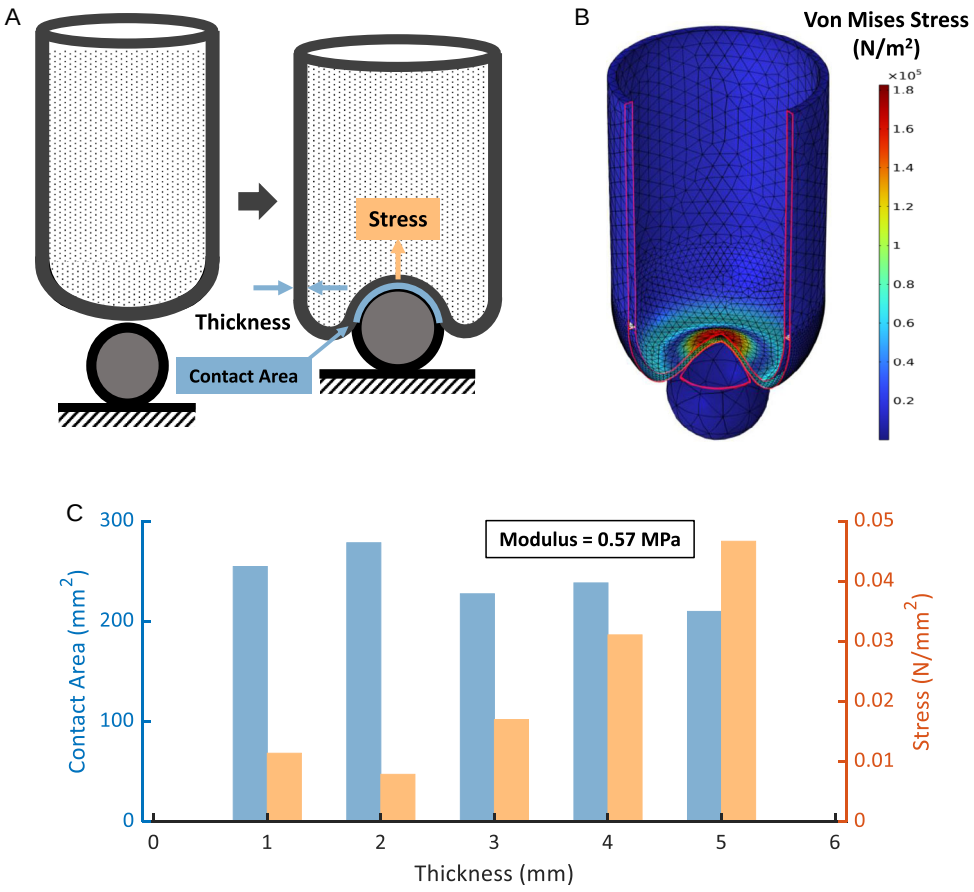

Figure 3. The FEA-based morphological optimization. A) Schematic of adaptive grasping, where the contact area and stress play key roles in the grasping performance. B) Cross-section view of an FEA simulation of the deformation in the SHUG upon adaptation to a spherical object with a diameter of 25 mm. C) The contact area and the stress as a function of the cover thickness for a fixed elasticity modulus of 0.57 MPa.

Table 2. Design parameters for the gripper.

Parameters	Values
Cylinder diameter	50 mm
Cylinder length	60 mm
Semisphere diameter	50 mm
Membrane thickness	2 mm
Membrane material	DPBM-FT3000-R05
Young's modulus	0.57 MPa

temperatures will lead to very long healing times and 2) too high temperatures will lead to degelation of the self-healing cover and the destruction of the gripper. Temperature is controlled in close loop via the integrated thermocouple; however, the heat transfer from the cartridge to the outer cover and the heat dissipation of the cover to the environment should be taken into account. Upon healing, the central heating element is activated and first heats up the surrounding metal balls. Due to the heat conductivity of the steel, the heat can be transported to the cover. Although having excellent conductivity, all steel granules will not be heated immediately, in particular due to porosity (i.e., gaps among particles). Meanwhile, there is heat dissipation between the outer layer of the self-healing cover and the atmosphere, thereby making the desired temperature (temperature on the outer surface of the DA membrane) difficult to control.

In this work, we modeled the heat transfer model as two thermal conduction and one thermal convection-cooling model. We assume that the solid thermal conductivity is radially isotropic and that the environment remains constant at ambient temperature, such that the dissipation phase is set as a fixed heat flux. We consider heat transfer in solids including the conduction through particles and the DA polymer, where the heat transfer in solids is governed by

$$\rho C_{\mathrm{p}}\left(\frac{\partial T}{\partial t}+\nu\cdot\nabla T\right)+\nabla q=Q_{\mathrm{t}}+Q_{\mathrm{h}} \tag{1}$$

where ρ (kg m^{-3}) and C_{p} (J (kg K)$^{-1}$) denote the solid density and heat capacity. ∇T and ν denote the temperature gradient (K m^{-1}) and velocity vector of translational motion (m s^{-1}). Q_{h} is the additional heat source from the central heating element (W m^{-3}) while $Q_{\mathrm{t}}=-\alpha T:\frac{dS}{dx}$ denotes the thermaelastic damping, indicating the thermoelastic effects in solids.[50] The heat flux by conduction (W m^{-2}) is denoted by $q=-k\nabla T$, where k is the solid thermal conductivity (W (m K)$^{-1}$). Based on experimental data, the parameters of the heat transfer from the DA polymer to the air, the intrinsic conduction coefficient of the DA material, and the thermal coefficients of the conduction among the "metal balls–gaps" hybrid are fitted.

Based on the thermal models, we simulated the heat transfer of the SHUG for an in-to-outside heating process (COMSOL Multiphysics). The heat transfer model is simulated in a 3D scenario with a central heating element. **Figure 4**B illustrates the steady-state contour distribution of temperature in a cross-section view. By measuring the variation of temperature gradient from the central heater to the outside surface of the membrane from three angles (0°, 45°, and 90°), the heat losses of the gripper are shown in Figure 4C. It can be seen that with a longer distance away from the cartridge heater, there is a decrease in temperature along the direction outward. Furthermore, the temperature in the dome area is slightly lower than in the side areas (0°). After the heat flux reaches the inner surface of the membrane, the temperature shows a dramatic drop until it reaches the exterior surface. In addition, the heat losses in three directions are in a tolerant range ($\leq$10°) such that it allows the SHUG interface to receive near-equal temperature treatment for SH and avoid local overheating.

2.3. Experimental Results

The grasping performance was first tested in a healthy condition by applying various levels of vacuum pressure while measuring the MHF using a tensile tester with a load cell. Next, we focused on hazardous grasping tasks and investigated the SHUG's effectiveness in resisting various types of damage. Then, the healing performance was investigated both on the material level and on the gripper level. The healing of the gripper was performed completely autonomously through precise temperature control. Finally, we demonstrated SHUG's reprocessability and recyclability from the perspective of economic sustainability.

2.3.1. Grasping Performance

Due to the particle jamming principle, the SHUG is able to grasp various objects with complex shapes. The grasping force is governed by both gripper and object attributes. On the gripper side, the selection of particles, membrane thickness, mechanical properties of polymers used for the cover, and vacuum pressure have a substantial impact on the grasp performance. From the object's perspective, the shape, size, texture, and roughness of the object, as well as the alignment of the gripper and the object, determine the firmness during adaptive grasping. Our proposed SHUG has been shown to be capable of grasping a range of objects, from irregularly shaped objects to common household objects (see Video S2, Supporting Information). **Figure 5**A demonstrates that a variety of different-shaped objects, including cylinders, spheres, cuboids, and hexagonal prisms, as well as a variety of complex-shaped everyday objects such as pliers, marking pens, and tapes, can be grabbed reliably in a pick-and-place task.

The SHUG's performance is characterized quantitatively, based on three experiments, by determining the MHF for objects with different shapes and sizes. All objects are fixed at the same position, while the SHUG is mounted on a tensile tester (Tinius Olsen 5ST) that moves the gripper up and down and measures the force using a load cell. During the experiment the SHUG moves downward and presses onto an object. Next vacuum is activated, resulting in particle jamming and the rigid state. Then the SHUG is instructed to move upward and the force is measured until the object is released from the gripper. **Figure 6**F depicts the holding force as a function of the distance the SHUG goes upwards for three different scenarios, including the pristine, the two recovered SHUG prototypes

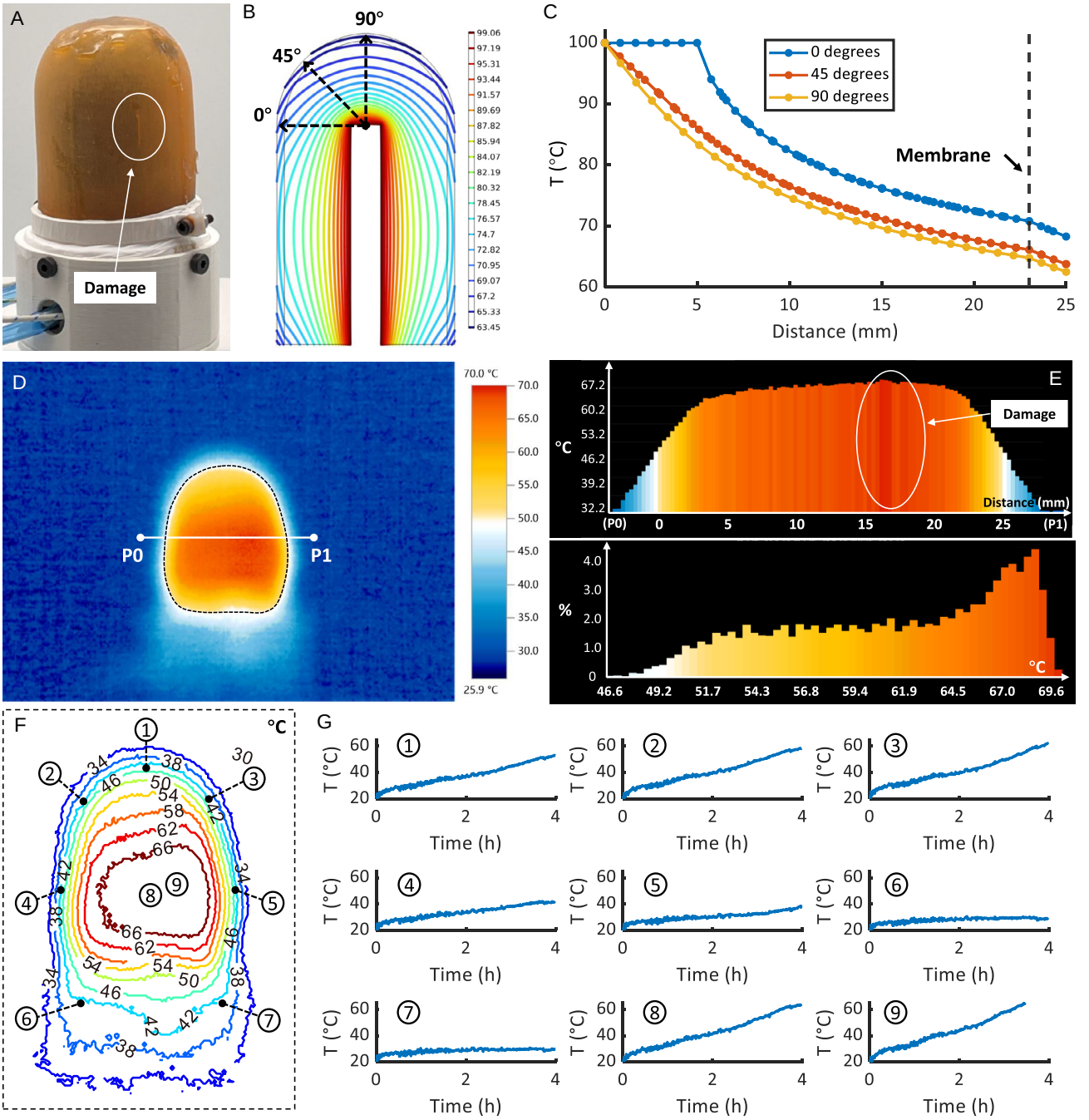

Figure 4. Heat regulation system. A) The real image of a damaged SHUG under the intrinsic heating treatment. B) Contour image of temperature in a cross-section view. C) Temperature gradients in three directions (0°, 45°, and 90°) in (B). D) Real-world temperature distribution on the SHUG surface captured by infrared thermal imaging camera. E) Temperature distribution from P0 to P1 (up) and temperature histogram (bottom) of the temperature isoline-curved (dashed) area in (D). F) The real image of the heating SHUG corresponds to (D). G) Temperature variation over time at nine different locations at the SHUG's interface.

after self-healing from puncture and scar damages. This force increases until reaching a plateau. At this plateau the MHF is reached. Due to the low lift velocity, the particle slightly flows around the object that is released and slips. Consequently we do not see a sudden grip. In this work, we consider the MHF as a key performance indicator for adaptive grasp as it indicates how much strength and reliability an object can be grasped.

In the first experiment, the shape of the object is varied, while the vacuum pressure is set at −50 kPa, and all the grasps are performed with the same intrusion distance (25 mm). The MHF is measured and compared for a cylinder, a cuboid, a hexagonal

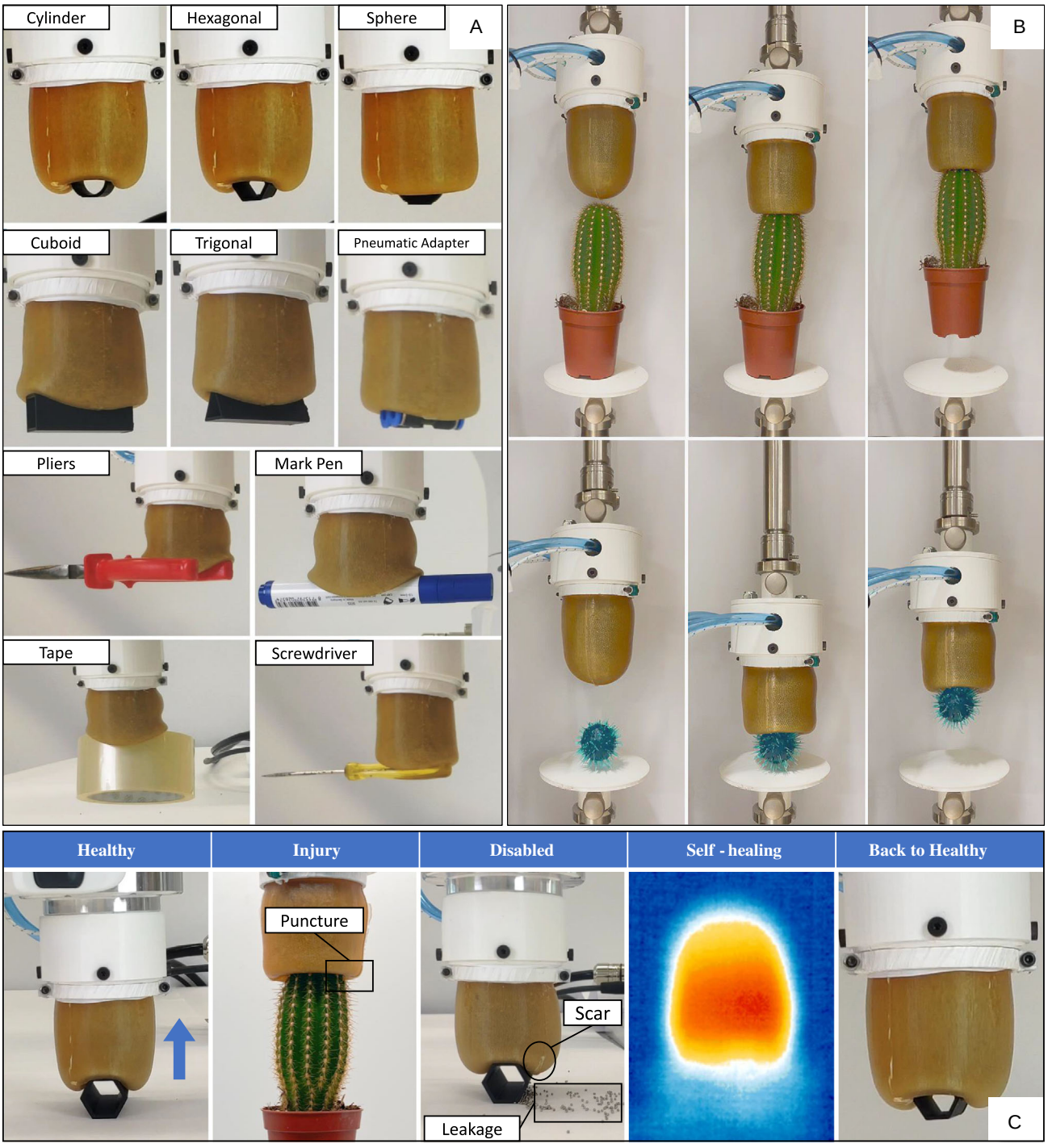

Figure 5. Universal adaptive grasping ability. A) The SHUG is versatile to grasp variously shaped and various daily used objects including pliers, marker pens, tapes, and screwdrivers. B) A three-stage time-series process of grasping hazardous objects such as a cactus (upper) and a thorned urchin (bottom), both imposing different levels of damage to the SHUG's interface. C) Five stages of SHUG's health rehabilitation from a hazardous grasp, during which the microscopic damage gradually propagates over time into perforations and leads to particle leakage, resulting in the disability of the SHUG. Subsequently, with autonomous damage detection and temperature treatment, the SHUG performs self-healing and recovers the mechanical properties.

prism, a triangular prism, a cube, and a sphere. Note that all the objects have the same width of 25 mm, which is half of the gripper's diameter size. Figure 6A illustrates that the MHF for all the objects is less than 3.5 N for the given condition. The adaptive grasp of the cuboid reaches the biggest MHF at 3.37 N among all the six geometric objects, while the triangular prism receives the smallest MHF (0.1 N). This change is determined by the contact area as well as by the orientation of the contact surfaces. The

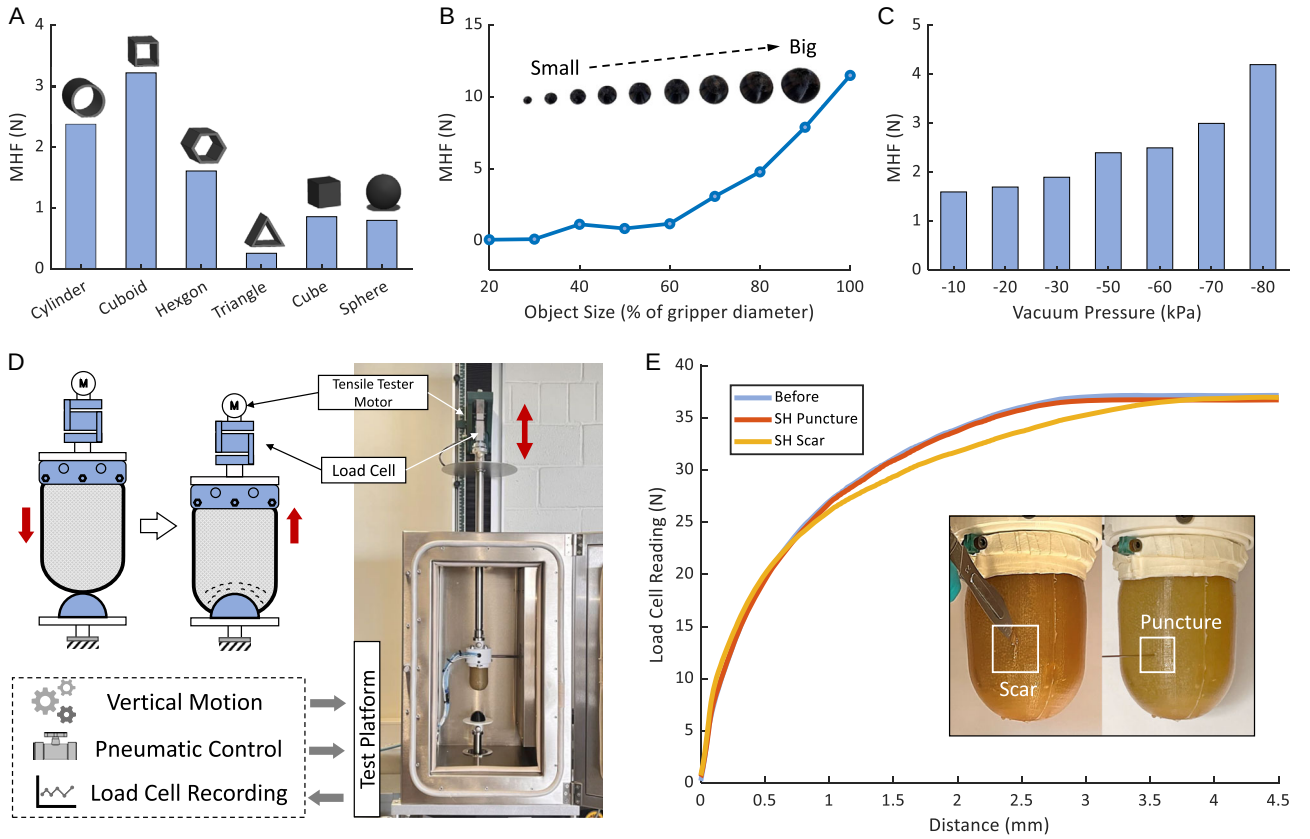

Figure 6. Holding force for the adaptive and resilient grasp. A) Maximum holding force versus various geometric-shaped objects. B) Maximum holding force versus varying-sized objects. C) Maximum holding force versus vacuum pressure. D) Schematic of the measurement of holding force with a load cell, with the SHUG mounted on a platform (tensile tester). The load cell reading is acquired during the pneumatic control of the grasping by the central computer, which also regulates the vertical motion of the gripper until contact with objects. E) The load cell readings in relation to the relative distance for three gripping scenarios, including an undamaged gripper, grippers that have self-healed from a puncture, and a scar. A needle and a scalpel are used to physically induce real damage (punctures and scars).

triangular prism is challenging[51,52] to grasp as the sharper angle pushed into the gripper makes it easier to slip out of the jammed interface. The proposed SHUG also achieves good performance for these highly convex-shaped objects.

For the second experiment, the SHUG grasps a hemisphere with varying sizes. The SHUG is pressed onto the hemisphere until it fully intrudes into the gripper. The MHF was derived for hemispheres with 20% to 100% the diameter of the gripper using a vacuum pressure of −80 kPa (the hemisphere with 10% of the gripper diameter cannot be gripped at all). Figure 6B shows that with increasing size, the MHF increases. For the largest hemisphere, whose diameter is the same as the one of the gripper, the MHF reaches 11.5 N. This results from the increase in the contact area. Consequently, very small objects, smaller than 30% of the grippers diameter, cannot be handled. The MHF is also influenced by the applied vacuum pressure. Using the SHUG to grasp a semisphere (80% of the gripper diameter) and by varying the vacuum pressure from −10 kPa to −80 kPa, the MHF as a function of the pressure is plotted in Figure 6C. The MHF gradually increases from 1.67 N at −10 kPa to 4.36 N at −80 kPa. A high vacuum results in a stronger particle jamming and consequently the object can be held more firmly.

2.3.2. Vulnerability of the Universal Gripper

As stated earlier, the gripper can be damaged as a result of hazardous working conditions in unstructured and unpredictable working environments. The SHUG can be damaged by sharp objects such as thorned plants, metal edges, shattered glass, and jagged plastics. To illustrate this, the SHUG was programmed to grasp a cactus and a thorned urchin (Figure 5B). Although the SHUG is able to manipulate these "dangerous" objects multiple times without macroscopic damage, punctures and leaks were created after a limited amount of grips (typically 2–6 grips). Three types of damages can be defined: 1) very large damages that lead to rupture of the cover and loss of particles and immediately impair the gripper's functionality; 2) damages that lead to the breakdown of the air tightness, causing the SHUG to fail to achieve full stiffness transition; and 3) small damages that do not lead to perforation but induce a scar, but pose a long-term threat as they can propagate over time into perforations. The latter situation was illustrated in an experiment in which a healthy SHUG grasped first a hexagon multiple times (20 grips), after which it picked up a cactus and continued grasping the hexagon. Although it was not damaged immediately, the SHUG was torn

after three grasps due to a small defect that propagated into the release of particles (Figure 5C). In the beginning, the minor damage may not immediately develop into a fatal failure to the gripper but with time the weak point is enlarged to a fatal scar, which may lead to particle leakage and the SHUG is no longer workable. Subsequently, with the autonomous damage detection and heat regulation (Figure 2B), the integrated system performs self-healing to allow the recovery of the interface's mechanical properties and the SHUG is finally back in a healthy condition.

2.3.3. Temperature Profile during Healing

Controlling the temperature in the SHUG is critical to perform the healing. Heating below 60 °C leads to limited mobility in the polymer network and a lack of sealing of microscopic cavities that results from slight misalignments of the fracture surfaces. Hence, the healing will not be completed and weak scars will be formed. Heating to very high temperatures, close to 110 °C, will degel the self-healing polymer, leading to a loss of structural stability and undesired flow of the cover. Therefore closed-loop temperature controls using the thermocouple and temperature loss compensation using the thermal model were needed.

To initiate the healing, the gripper is placed in its healing position, with the tip facing upwards. This is to maximize the contact between the conductive particles with the Joule heater and also let the PLA holding base instead of the soft membrane support the metal granules. The internal cartridge is heated to 100 °C, which results in equilibrium to a temperature at the exterior of the cover of around 70 °C, according to the thermal simulation. The temperature distribution evolution during heating is investigated by a time-series infrared image of a damaged SHUG during the healing process (Video S5, Supporting Information). For this experiment, the SHUG was damaged by a scalpel blade at the location marked with "*x*" in **Figure 7**B. It validates that the outer surface of the cover of the SHUG can be intrinsically heated from room temperature to the designed healing temperature (70 °C). However, this takes time. Figure 4G depicts the evolution of the temperature at different locations on the SHUG interface, indicated in Figure 4F. Due to its thermal mass it takes the SHUG prototype roughly 4 h to reach a temperature around 60–70 °C in the outer layer of its cover. This heating time can be reduced by integrating a larger heating device and using a varying temperature profile in the heater. However, care should be taken as increasing the temperature too extensively will lead to the destruction of the gripper. After this 4 h healing procedure, all damages described in the article could be healed entirely, restoring the gripper's full performance

Figure 4D shows the actual temperature distribution on the SHUG captured by an infrared thermal imaging camera (Testo). This confirms that the gripper's exterior surface reaches the desired temperature range of 60–70 °C. It also demonstrates that the temperature distribution in the dome region is slightly lower than in the side region, which is in line with the theoretical simulation results in Figure 4C. Figure 4E illustrates the temperature distribution in a directed line segment (*P*0 to *P*1 in 4D) and the histogram of temperature in the region of the isothermal curve (dashed curve area in 4D) in the ground-truth thermal image, respectively. Figure 4A shows the real image of the gripper in a health-repairing process corresponding to 4D. Note that before the self-healing process, the gripper is damaged with a local cut at the center-right interface. The higher temperature observed at the damaged area is due to a higher heat transfer coefficient for steel-to-air convection compared to polymer-to-air convection (see Figure 4E).

Operating environmental temperatures can influence the performance of the gripper. Although being mechanically stable, the mechanical behavior does change depending on the operating temperature. In application temperatures that are typical for soft grippers (from –5 to 40 °C), these changes are rather small. In addition, these changes affect the material behavior; however, as the operation of the gripper relies on jamming, rather than on a controlled elastic deformation, its operation will not be changed substantially. At higher temperatures the materials mobility increases and it becomes flexible. Therefore, the gripper will be slightly more adaptive to the shape of an object prior to jamming. The glass transition temperature of the material is at −44 °C. Consequently, the gripper can be used in cold environments which typically do not go to these extremes.

2.3.4. Self-Healing Performance

As a first nonquantitative illustration of the healing ability, the damages caused by the cactus were healed autonomously via internal heating. The gripper starts the self-healing program, by positioning itself into its healing orientation. The gripper rotates prior to heating, because at higher temperatures the self-healing material is slightly softer, due to the decrease in DA crosslinks. Consequently, the gripper's resistance to plastic deformation due to the heavy weight of the steel balls is slightly decreased. With the tip pointing upward, the steel balls exert their weight on the PLA part. Next, the heating element increases the temperature in the gripper following the heat regulation illustrated in Figure 4, leading to the repair of the damage, as the gripper regains air tightness. Finally, the gripper returns to a healthy working condition and is able to continue grasping (Figure 5C).

In order to have good control over the healing in the SHUG, the healing temperature and healing speed have to be investigated on the material level. A self-healing polymer sheet (thickness of 2 mm) was manually cut using a scalpel blade (**Figure 8**A). The damaged sample was placed under an optical microscope and onto a heating plate (see Video S4, Supporting Information). Although elastic recovery brings the fracture surfaces back in contact, microscopic gaps, like the one seen here, can remain present. The heater plate was heated at 10 K min^{-1} starting at room temperature, while the microscopic images were recovered to visualize the self-healing procedure (Figure 7C). As illustrated by the time series, the polymer heals from the scalpel cut. The length of the damage is also plotted as a function of time, together with the temperature profile in Figure 7A. It takes about 9 min to completely seal the microscopic damage. There is no closure/sealing registered before reaching temperatures of 70 °C. At lower temperatures, the mobility in the polymer network, which is needed to seal

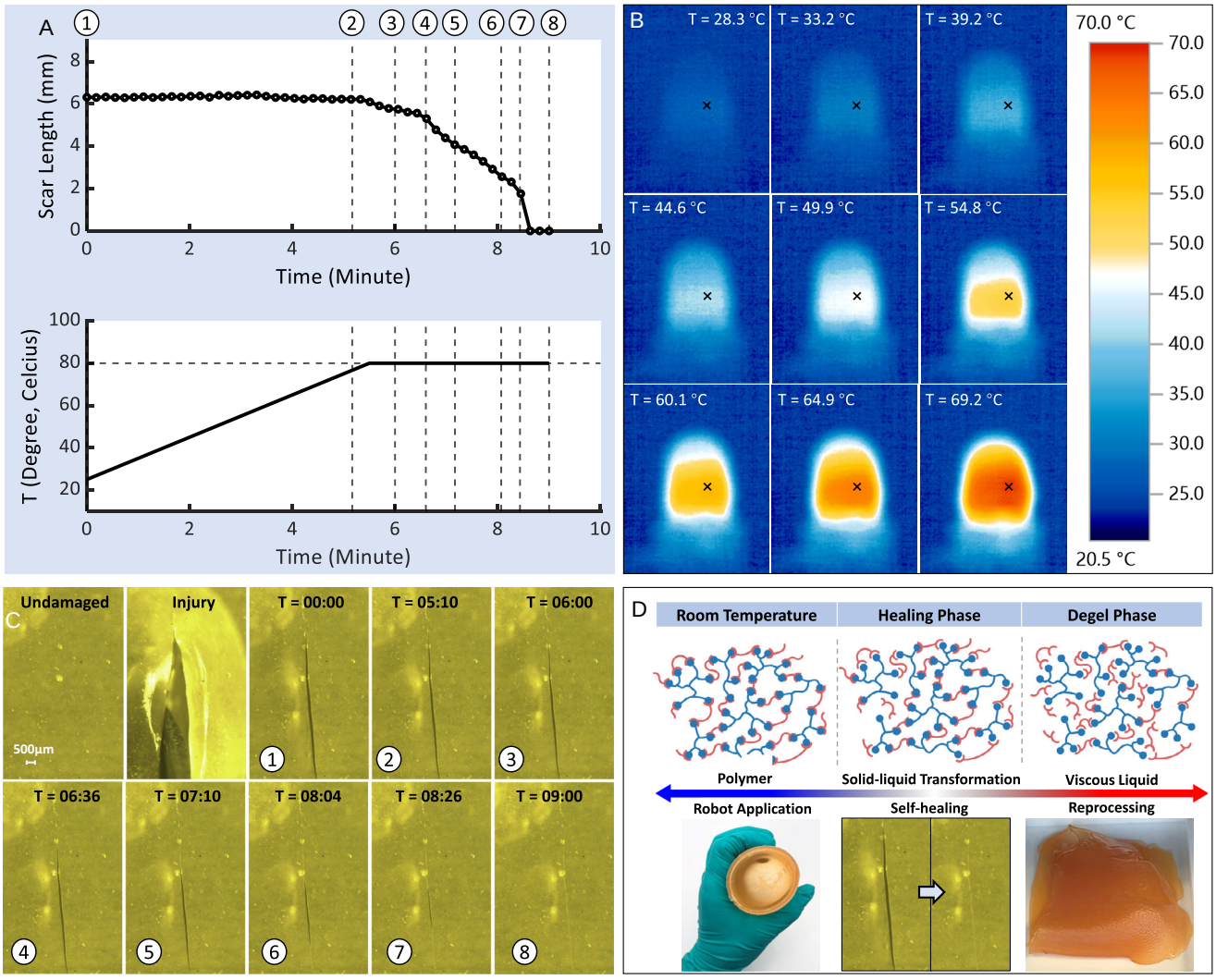

Figure 7. Self-healing efficiency for DA material (DPBM-FT5000-R05) and the gripper. A) Scar length of the damaged material over time, where the polymer heals completely after 9 min. The bottom subplot shows the controlled temperature treatment from a heating plate. B) Time-series infrared images of the temperature variation on the SHUG from room temperature to a desired healing temperature, where the temperature at the damaged point is probed. C) Time-series images (corresponding to eight stages in (A)) of a damaged DA polymer self-heals from a macroscopic scratch. D) The elastomeric network has reversible solid–liquid transformation under regulated temperature treatment. At low temperatures, the network is produced due to strong conversion to DA bonds; however, at high temperatures, the DA bonds break apart and the mobility of the polymer chains increases.

damages, is not present. Consequently, the healing in the SHUG is desired to be performed at 70 °C. It should be noted that, while the damage has been completely sealed, it has not yet completely healed. For the material to recover its initial mechanical properties, the polymer has to be cooled down to room temperature, during which the DA crosslinks are reformed in the network and across the fracture surfaces, as shown in the self-healing cycle in Figure 10.

We summarized four types of common damage that can occur in the cover and to investigate the healing performance quantitatively, these four types of damages were replicated on DPBM-FT3000-r0.5 material samples ($30 \times 5 \times 2\ mm^3$). As illustrated in Figure 8A, a scalpel is used to notch the surface to mimic the damages caused by sharp objects or jagged edges. The sheet is pierced by a needle to replicate the damages posed by thorny objects such as broken glass and spiky twigs. The cut and tear attempt to duplicate the fatal damages to the gripper when a large deformation occurs during the adaptation to a sharp object, as this leads to catastrophic failure of the soft gripper. Small damages like superficial cuts and needle punctures receive an automatic alignment as the elastic deformation brought the fracture surfaces back in contact (Video S3, Supporting Information). For large damages, like cuts and tears, the fracture surfaces are brought back in contact manually. However, we observed that in the gripper, even these large cuts and tears were sealed autonomously through the elastic recovery of the self-healing elastomer. After recontact, the samples were heated in a preheated oven at 70° for 30 min. Next, the samples were tested in a tensile test until fracture with a strain ramp of 1 1% s^{-1} and compared to the stress–strain characteristic of a

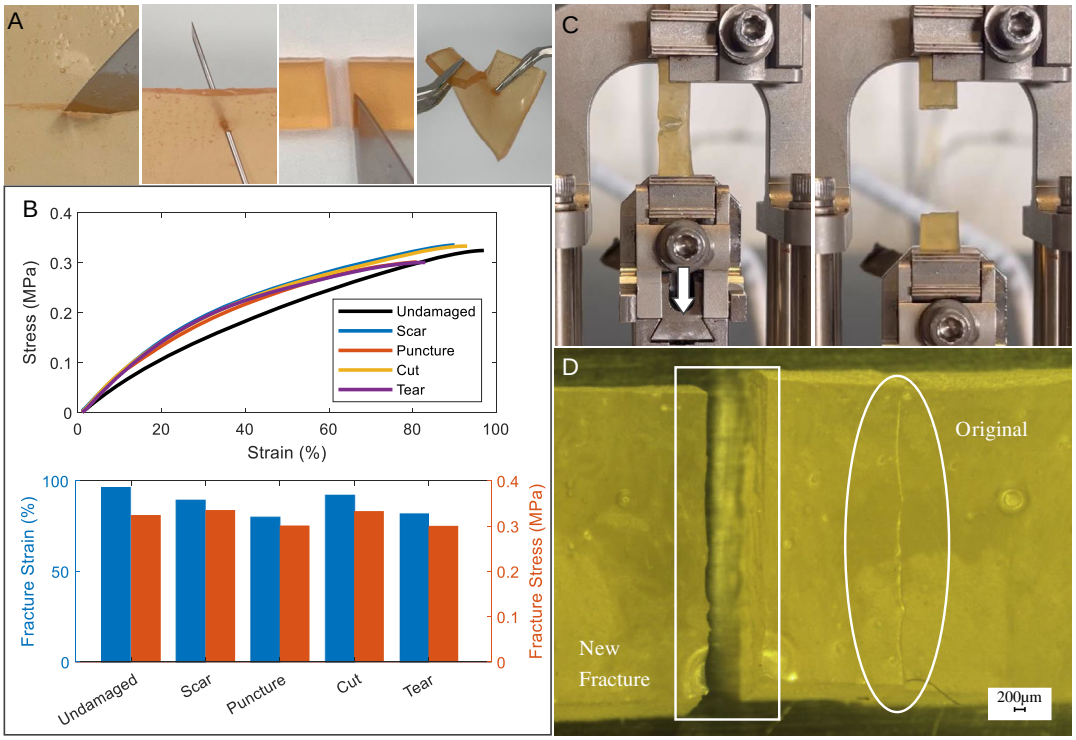

Figure 8. The DA membrane is able to self-heal from various macroscopic damages. A) Four types of damages including (left to right) scratch, puncture, cut, and tear. B) The comparison of stress–strain curve and elongation rate for the DPBM-FT3000-R05 sample before and after the self-healing. C) The axial normal stress and strain measurement in a tension test. D) For a healed sample, the original damaged part is no longer a weak point.

pristine sample (Figure 8B). It is clear that after healing, a very large part of the mechanical properties, including Young's modulus, fracture stress, and fracture strain, is recovered.

The high healing efficiencies, based on the recovery of Young's modulus, fracture stress, and fracture strain, illustrate the excellent healing capacity of the self-healing polymer. This is emphasized by microscopic analysis of the sample that was healed from being cut in two and fractured in the tensile test (Figure 8C). On the microscopic image, it can be seen that the new fracture occurred at a location that differs from the original scar. This means that during the healing procedure of the detached two parts, the mechanical properties were completely recovered and there was not a weak point (Figure 8D) created at the location of the scar. This procedure had been repeated for 5 times and showed each time the same result. However, in practical industrial applications, the same damages can occur repeatedly at the same spot. Nevertheless, not only the mechanical properties are recovered after healing, also the healing capacity at the location of the scar is recovered using this material-based healing. However, contamination is one concern that needs to be taken in account in future applications. If the damaged interface is fractured with unclean sharp items, contamination from these objects may impede the reformation of the covalent network via DA covalent bonds, thus reducing the material's self-healing capabilities.

The healing performance was measured on the gripper level. The holding force was measured during grasping of a hemisphere (80% of the gripper's diameter) with a vacuum pressure of −80 kPa on an undamaged SHUG as a reference, and before and after healing a puncture that was made with a needle and a scalpel cut in the gripper's interface. Due to loss of air tightness the damaged gripper could not generate any holding force. The two damages were healed at over 4 h following the health regulation and temperature profiles. It can be seen from Figure 6E that overall the contact forces in three cases increase very similarly as a function of the distance traveled by the tensile tester, before reaching a plateau at the force of 40 N. It is clear that also on the gripper level damages can be healed and the gripper's performance can be almost completely recovered. Small deviations in the MHF can be attributed to small differences in the adaptation of the membrane around the object or the positioning of the particles in the SHUG during the experiment.

2.3.5. Reprocessing and Recycling of the SHUG

In the case of very large cuts or fractures (as depicted in **Figure 9**A) and the loss of materials, we advise against attempting self-healing. Instead, it is recommended to remove the damaged soft cover from the gripper and recycle it to create a new one. Realignment of the fracture surfaces cannot be done without human intervention, making recycling a more practical and efficient option. The produced SHUG is not only healable but it is also manufactured completely out of polymers that can be recycled via mechanical reprocessing. The PLA parts can be shredded and created into filament through single-screw extrusion which can be again used for fused filament fabrication

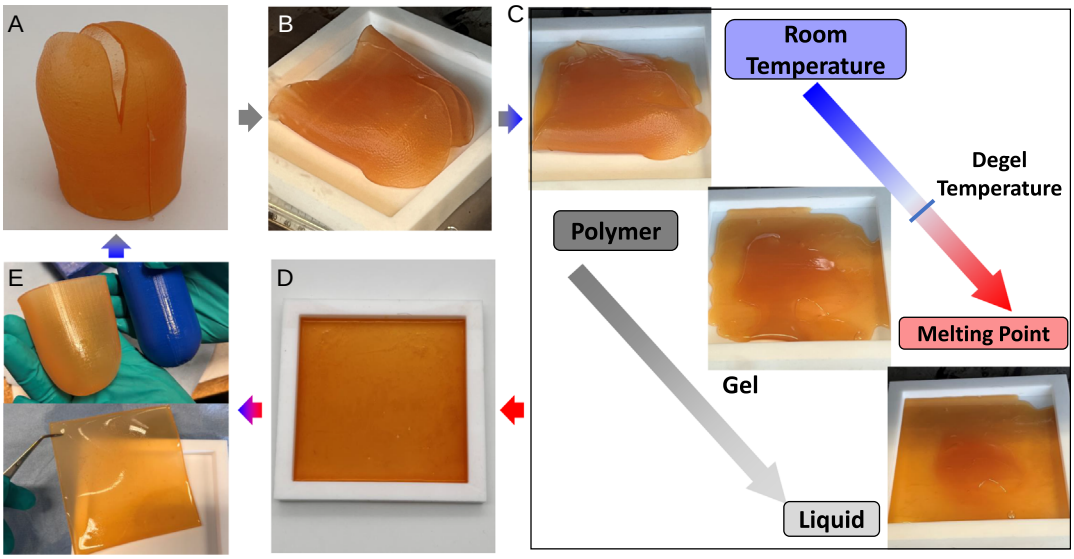

Figure 9. Recyclability and sustainability of the SHUG. A) The deformable SH membrane has been fatally damaged and removed from the SHUG prototype, after which B) the cover has been cleaned, washed, dried, and placed onto a Teflon container. C) With a controlled temperature treatment in oven, the polymer has been degelled and transformed to viscous flow. D) After an isothermal temperature treatment, the melted DA polymer exhibits homogeneous mechanical properties, after which E) the vicious flow can be either reprocessed for mold casting or sample sheets.

printing. The steel balls can be reused in a new gripper or can be reprocessed through melting. In high contrast with conventional materials used in soft robotics, for example, silicones, the self-healing polymer can be reprocessed through heat treatment. By heating the polymer above its degelation temperature (110 °C), it exhibits a viscous flow behavior in which it can be reprocessed. To illustrate its reprocessing capacity, a cover that was severely damaged was degelled by heating it in an oven at 150 °C (Figure 9). The resulting viscous liquid polymer was recast in the PLA mold to create a new self-healing cover. As depicted in Figure 9E, the recycled DA polymer was employed to produce a new soft cover through mold casting. This new cover was used on the robotic arm and showed no change in performance compared to the pristine cover. This is in line with observations in previous work that showed that reprocessing hardly changes the mechanical properties of the self-healing polymer or its healing capacity.[45]

3. Discussion

In this article we proposed the SHUG, developed for its adaptive grasp and its resilience to damage when operating in unknown, complex, or/and hazardous environments. The gripper is based on the particle jamming principle and can perform gripping tasks for a wide variety of arbitrarily shaped objects. The vulnerable component, the flexible cover, is manufactured from self-healing polymers, integrating a healing ability in the soft gripper. For this we used reversible DA polymers, which combine excellent mechanical strength with reliable healing at moderated temperatures (60–70 °C). The entire healing process, which requires heat, was automatized by embedding a controlled heater in the gripper. Before physical fabrication and experimentation, its design was optimized via an FEA-based optimization, in which the most appropriate cover thickness and mechanical strength were defined. Model-driven design and optimization reduced the workload and expense prior to physical experimentation with an acceptable sim-to-real gap. In addition, steel balls were selected as in-filled particles via optimizing a combination of adequate density, fluidity, and thermal conductivity. The latter is important for the heat transfer from the embedded heater toward the outer cover during heat-assistive healing.

The SHUG is manufactured via a new solvent-less two-step synthesis and casting. Inside of the gripper, in between the steel balls a heat cartridge provides the heat that is transferred to the self-healing cover via the highly conductive steel balls. Using a thermocouple, a closed-loop temperature controller was integrated that takes in account the heat distribution during healing via a heat transfer model. As such the healing can be performed completely autonomously without any external intervention. The authors believe that autonomous healing is key in developing resilient systems, as external intervention vastly increases the cost of healing. Practical grasping experiments have shown that the SHUG is able to perform pick-and-place tasks for various objects and the soft cover can heal from a series of damages, ranging from local small damage, including scratch and puncture, to fatal damage such as cut and tear and this is completely autonomous using the proposed health regulatory framework.

The healing capacity can be an enabling technology for soft grippers like the universal gripper in applications where sharp objects and edges lead to damage after a limited number of grasping cycles. Being able to recover from damages increases the competitiveness of soft grippers in these applications and increases their sustainability. The latter is enhanced by the illustrated recyclability of the entire gripper, which is in high contrast with the traditional silicones currently used in soft robotic grippers.

4. Experimental Section

Principle of Reversible Elastomeric Network: The self-healing material is based on the DA crosslinks in the polymer network. The DA reaction describes the reversible cyclo-addition reaction of a diene (here furan) and a dienophile (here maleimide) with outcome as DA adduct (Figure 2C).[53] Being an equilibrium reaction, it contains the forward DA reaction (bond formation) and the retro-DA reaction (bond breaking). Upon heating, the retro-DA reaction is favored, leading to a decrease in crosslinks and an increase of unreacted maleimide and furan in the polymer network, leading to an increase in mobility and reactivity. At high temperatures (70–80 °C), this increase in mobility does not lead to a loss of mechanical stability and the material remains solid; however, combined with the increased reactivity it allows to perform healing in an acceptable period (e.g., 1 h).

Upon heating to higher temperatures, above the degelation temperature (>120 °C), extensive breaking of the DA crosslinks leads to a loss of the polymer network structure and structural stability, leading to viscous flow. In this liquid state the material can be reprocessed. Upon cooling the DA reaction is favored, leading to a full recovery of the polymer network structure and the initial material properties. This is in strong contrast with traditional elastomers used in robotics (e.g., silicone), as their network is irreversibly formed during synthesis. Consequently, upon heating these elastomers do not flow before degradation and hence cannot be reprocessed.

Self-Healing Procedure: The healing in the DA polymers consists of five stages (**Figure 10**). 1) Upon damage, locally at the location of damage DA bonds are broken as these are the weakest covalent bonds in the network. Throughout the network, the crosslinks remain intact. 2) The fracture surfaces are brought back in contact, through internal elastic recovery or via external intervention. 3) To enable self-healing, the polymer is heated to 70 °C, which shifts the equilibrium of the DA reaction to the unbound state. The generated dangling chains with reactive maleimide or furan lead to an increase in reactivity and in mobility in the network; however, the polymer remains in the solid state. 4) Remaining at this temperature for some time allows to seal the microscopic gap and rebind across the fracture surface. 5) Decreasing the temperature to ambient conditions pushes the equilibrium of the DA reaction back to the bound state, recovering the initial number of crosslinks throughout the network as well as across the fracture surfaces. The result is a sample or part which is as good as new, having the same initial material properties as prior to the damage.

Monomer Materials: The triamine Jeffamines T3000 has trifunctional polypropylene glycol backbones and an average molar mass of 3240 g mol^{-1} and was supplied by Huntsmann (Belgium). Furfuryl glycidyl ether (FGE), with a purity of 95%, was purchased from Sage Chemicals (China) and stored in refrigerated conditions. 1,1-(Methylenedi-4,1-phenylene)-bismaleimide (DPBM), with a purity of 95% and a molar mass per functionality (M_M) of 189 g mol^{-1}, was obtained from Sage Chemicals (China). 4-*tert*-butylcatechol was used as a radical inhibitor and was supplied by Sigma-Aldrich. The chemicals utilized in the study were employed as delivered. The chemical structure of these reagents can be found in Supporting Information.

Synthesis and Polymer Network Composition: The self-healing polymers were synthesized in a two-step, solvent-less synthesis. First, FGE reacted with a stoichiometric amount of Jeffamine, yielding a furan-functionalized Jeffamine (FT3000) compound with a molar per functionality (M_F) of 691 g mol^{-1} (**Figure 11**: Stage 1). The irreversible reaction was performed for a minimum of 7 days at 60 °C under continuous magnetic stirring, after which the reaction was completed for 2 days at 90 °C.

Next, the network was synthesized through the mixing of FT3000 and DPBM and crosslinking via the DA reaction (Figure 11: Stage 2). In previous work, solvent casting using chloroform was used to synthesize sheets of self-healing polymers. As DPBM in its crystalline state cannot be dissolved in FT3000, DPBM, 4-*tert*-butylcatechol crystals (5 wt% of DPBM), and FT3000 were first dissolved in chloroform (20 wt%) through magnetic stirring at 25 °C for 24 h. 4-*tert*-butylcatechol was used as the radical inhibitor to prevent an undesired side reaction at high temperatures, for example, the homopolymerization of maleimide, which leads to a loss of the healing ability. The chloroform was evaporated through solvent casting under vacuum at 25 °C for 24 h. Upon solvent evaporation, the concentration of maleimide and furan increased, pushing the equilibrium of the DA toward the bond state, resulting in the formation of the polymer network.

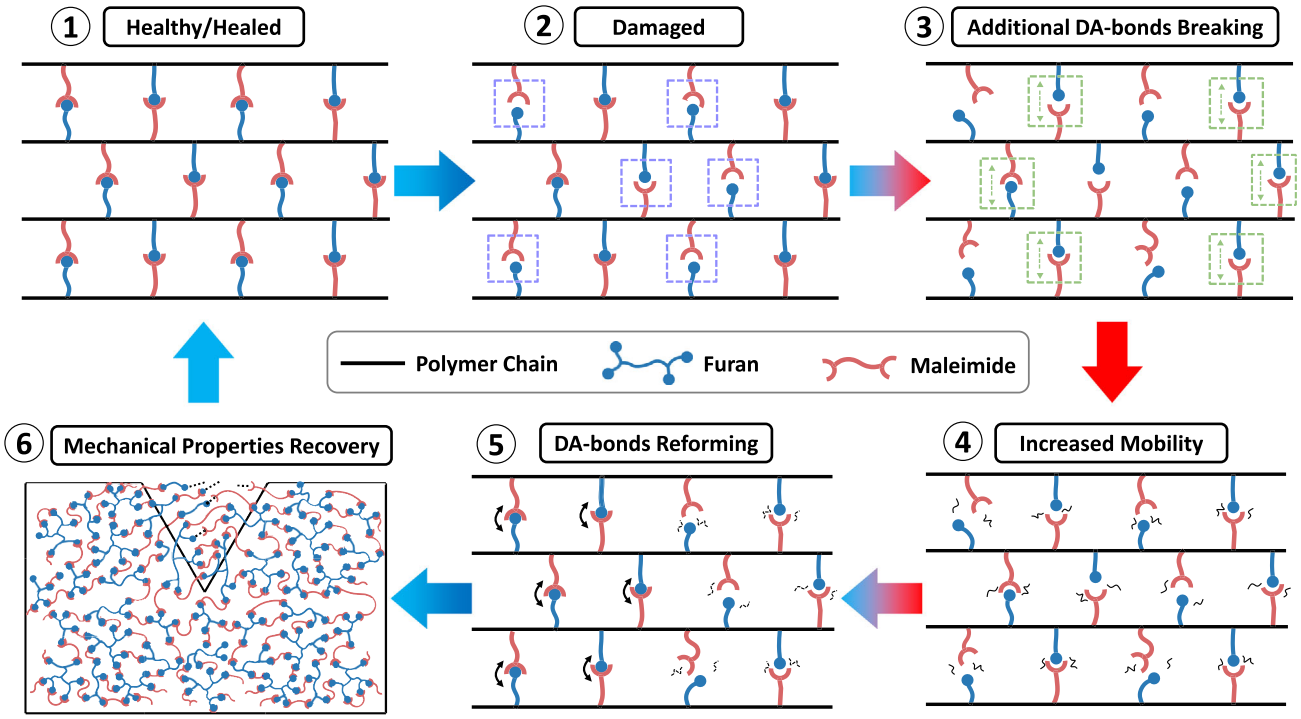

Figure 10. The self-healing heat–cool cycle of the DA polymer and the accompanying illustrations of the DA reversible process.

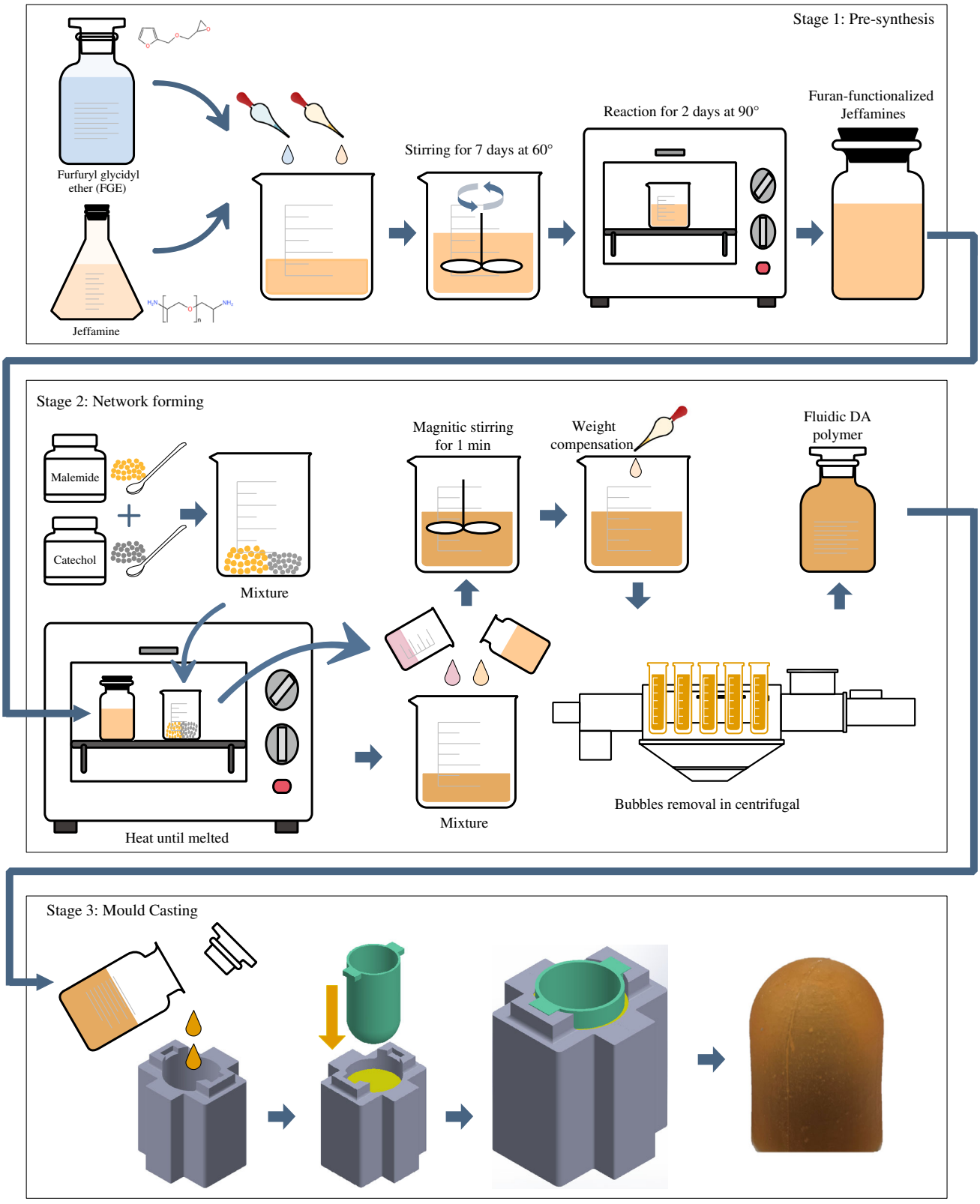

Figure 11. Flowchart of the fabrication of the self-healing membrane.

However, this synthesis is time consuming and uses the carcinogenic chloroform, which can easily access the human body via skin or respiration.

In this work, we developed a new fast and solvent-less synthesis. We first melted the DPBM crystals (with a melting point of 155 °C) alongside 4-*tert*-butylcatechol crystals (5 wt% of DPBM, with a melting point at 50 °C) at 160 °C to enhance their solubility. Next hot FT3000 (at 160 °C) was added with an off-stoichiometric maleimide-to-furan ratio of 0.5 ($r = [M_0]/[F_0]$, with $[M_0]$ and $[F_0]$ the maleimide and furan concentrations). To synthesize material with a total mass of m_t, following masses of FT5000 (m_F) and DPBM (m_M) were needed.

$$\begin{aligned} m_M &= \frac{m_t}{\frac{1}{r}\frac{M_F}{M_M} + 1} \\ m_F &= \frac{m_t}{r\frac{M_M}{M_F} + 1} \end{aligned} \tag{2}$$

where r is the stoichiometric malimide-to-furan ratio (unitless) and M_M and M_F are the average molar masses per functionality of DPBM and FT3000, respectively (g mol^{-1}).

Immediately after pouring the hot FT5000 on the DPBM melt, the parts were mixed for 1 min using a magnetic stirrer. Bubbles that were induced by mixing were removed by inserting the mixture in an Eppendorf Centrifuge 5804 at 5000 rpm for 2 min. Afterward, the degassed mixture was cast in an appropriate mold to form testing samples or the SHUG (Figure 11: Stage 3). The mixture reacted into a DPBM-FT3000-r0.5 elastomer due to DA crosslinking. After 24 h at ambient conditions, the polymer network was completely formed and stable material properties were reached. Due to the low maleimide-to-furan ratio, $r = 0.5$, there was an excess of furan present in the polymer network. As illustrated in previous work,[45,54] this excess increased the reaction rate of the DA reaction, leading to faster healing at low temperatures. Consequently, this low r value was selected in this work.

Experimental Setups for Polymer and Prototype Characterization: The mechanical characteristics of the Diels-Alder polymer, prior to damage and after healing, were examined via tensile testing on a TA Instruments Q800 dynamic mechanical analyzer (DMA). The MHF of the SHUG for different objects was measured on a single-axial tensile tester (Tinius Olsen 5ST) at room temperature (25 °C). A pressure pump powered the SHUG. This pressure was converted into vacuum via SMC ZH10DSA vacuum ejector. The vacuum was controlled via a SMC IRV10-N07 regulator. Relative to atmospheric pressure, the vacuum pressure ranged from 0 to −100 kPa. To further test the SHUG's functionality, the gripper was placed as an end effector on a 6-DoF robot manipulator (Franka Emika).

Supporting Information

Supporting Information is available from the Wiley Online Library or from the author.

Acknowledgements

This project received funding from the EU Marie Sklodowska-Curie SMART Project (no. 860108). The Fonds Wetenschappelijk Onderzoek (FWO) funded the work through personal grant to S.T. (1100416N). Z.W. was funded by China Scholarship Council (CSC).

Conflict of Interest

The authors declare no conflict of interest.

Author Contributions

H.W. and Z.W. took care of visualization. G.V.A., F.I., and B.V. took care of funding acquisition. F.I. and B.V. took care of project administration. G.V.A., F.I., and B.V. took care of supervision. H.W. took care of writing the original draft. H.W., S.T., F.I., and B.V took care of writing the review.

Data Availability Statement

The data that support the findings of this study are available from the corresponding author upon reasonable request.

Keywords

adaptive grasp, Diels–Alder polymers, self-healing materials, soft robotics, universal grippers

Received: May 3, 2023
Revised: July 6, 2023
Published online: August 29, 2023

[1] J. Amend, N. Cheng, S. Fakhouri, B. Culley, *Soft Rob.* **2016**, *3*, 213.
[2] B. Ward-Cherrier, N. Pestell, L. Cramphorn, B. Winstone, M. E. Giannaccini, J. Rossiter, N. F. Lepora, *Soft Rob.* **2018**, *5*, 216.
[3] E. Brown, N. Rodenberg, J. Amend, A. Mozeika, E. Steltz, M. R. Zakin, H. Lipson, H. M. Jaeger, *Proc. Natl. Acad. Sci. USA* **2010**, *107*, 18809.
[4] L. Zhou, L. Ren, Y. Chen, S. Niu, Z. Han, L. Ren, *Adv. Sci.* **2021**, *8*, 2002017.
[5] J. Shintake, V. Cacucciolo, D. Floreano, H. Shea, *Adv. Mater.* **2018**, *30*, 1707035.
[6] T. Jin, T. Wang, Q. Xiong, Y. Tian, L. Li, Q. Zhang, C.-H. Yeow, *Soft Rob.* **2023**, *10*, 785.
[7] C. Linghu, S. Zhang, C. Wang, K. Yu, C. Li, Y. Zeng, H. Zhu, X. Jin, Z. You, J. Song, *Sci. Adv.* **2020**, *6*, eaay5120.
[8] J. R. Amend, E. Brown, N. Rodenberg, H. M. Jaeger, H. Lipson, *IEEE Trans. Rob.* **2012**, *28*, 341.
[9] N. F. Lepora, Y. Lin, B. Money-Coomes, J. Lloyd, *IEEE Rob. Autom. Lett.* **2022**, *7*, 9382.
[10] R. Pfeifer, M. Lungarella, F. Iida, *Science* **2007**, *318*, 1088.
[11] C. A. Aubin, B. Gorissen, E. Milana, P. R. Buskohl, N. Lazarus, G. A. Slipher, C. Keplinger, J. Bongard, F. Iida, J. A. Lewis, R. F. Shepherd, *Nature* **2022**, *602*, 393.
[12] S. Song, D.-M. Drotlef, D. Son, A. Koivikko, M. Sitti, *Adv. Sci.* **2021**, *8*, 2100641.
[13] C. Majidi, *Adv. Mater. Technol.* **2019**, *4*, 1800477.
[14] Y. Zhang, W. Zhang, P. Gao, X. Zhong, W. Pu, *Nat. Commun.* **2022**, *13*, 7700.
[15] Y. Lin, C. Zhang, W. Tang, Z. Jiao, J. Wang, W. Wang, Y. Zhong, P. Zhu, Y. Hu, H. Yang, J. Zou, *Adv. Sci.* **2021**, *8*, 2102539.
[16] T. Wallin, J. Pikul, R. Shepherd, *Nat. Rev. Mater.* **2018**, *3*, 84.
[17] U. Kim, D. Jung, H. Jeong, J. Park, H.-M. Jung, J. Cheong, H. R. Choi, H. Do, C. Park, , *Nat. Commun.* **2021**, *12*, 7177.
[18] D. Rus, M. T. Tolley, *Nature* **2015**, *521*, 467.
[19] S. Kim, C. Laschi, B. Trimmer, *Trends Biotechnol.* **2013**, *31*, 287.
[20] C. F. Guimarães, L. Gasperini, A. P. Marques, R. L. Reis, *Nat. Rev. Mater.* **2020**, *5*, 351.
[21] R. V. Martinez, A. C. Glavan, C. Keplinger, A. I. Oyetibo, G. M. Whitesides, *Adv. Funct. Mater.* **2014**, *24*, 3003.
[22] W. Liu, Y. Duo, J. Liu, F. Yuan, L. Li, L. Li, G. Wang, B. Chen, S. Wang, H. Yang, Y. Liu, Y. Mo, Y. Wang, B. Fang, F. Sun, X. Ding, C. Zhang, L. Wen, *Nat. Commun.* **2022**, *13*, 5030.

[23] M. Wu, X. Zheng, R. Liu, N. Hou, W. H. Afridi, R. H. Afridi, X. Guo, J. Wu, C. Wang, G. Xie, *Adv. Sci.* **2022**, *9*, 2104382.
[24] J. Hughes, U. Culha, F. Giardina, F. Guenther, A. Rosendo, F. Iida, *Front. Rob. AI* **2016**, *3*, 69.
[25] R. Deimel, O. Brock, *Int. J. Rob. Res.* **2016**, *35*, 161.
[26] S. Terryn, J. Langenbach, E. Roels, J. Brancart, C. Bakkali-Hassani, Q.-A. Poutrel, A. Georgopoulou, T. George Thuruthel, A. Safaei, P. Ferrentino, T. Sebastian, S. Norvez, F. Iida, A. W. Bosman, F. Tournilhac, F. Clemens, G. Van Assche, B. Vanderborght, *Mater. Today* **2021**, *47*, 187.
[27] R. A. Bilodeau, R. K. Kramer, *Front. Rob. AI* **2017**, *4*, 48.
[28] Y. J. Tan, G. J. Susanto, H. P. Anwar Ali, B. C. Tee, *Adv. Mater.* **2021**, *33*, 2002800.
[29] Y. Yan, Z. Hu, Z. Yang, W. Yuan, C. Song, J. Pan, Y. Shen, *Sci. Rob.* **2021**, *6*, eabc8801.
[30] J. Xiong, J. Chen, P. S. Lee, *Adv. Mater.* **2021**, *33*, 2002640.
[31] M. Khatib, O. Zohar, H. Haick, *Adv. Mater.* **2021**, *33*, 2004190.
[32] D. Hardman, T. George Thuruthel, F. Iida, *NPG Asia Mater.* **2022**, *14*, 11.
[33] J. Ge, X. Wang, M. Drack, O. Volkov, M. Liang, G. S. Cañón Bermúdez, R. Illing, C. Wang, S. Zhou, J. Fassbender, M. Kaltenbrunner, D. Makarov, *Nat. Commun.* **2019**, *10*, 4405.
[34] X. Le, W. Lu, J. Zhang, T. Chen, *Adv. Sci.* **2019**, *6*, 1801584.
[35] P. Ferrentino, A. Lopez-Diaz, S. Terryn, J. Legrand, J. Brancart, G. Van Assche, E. Vazquez, A. Vazquez, B. Vanderborght, *IEEE Rob. Autom. Lett.* **2022**, *7*, 7391.
[36] F. Herbst, D. Döhler, P. Michael, W. H. Binder, *Macromol. Rapid Commun.* **2013**, *34*, 203.
[37] J. Cui, A. del Campo, *Chem. Commun.* **2012**, *48*, 9302.
[38] P. Cordier, F. Tournilhac, C. Soulié-Ziakovic, L. Leibler, *Nature* **2008**, *451*, 977.
[39] S. Burattini, H. M. Colquhoun, J. D. Fox, D. Friedmann, B. W. Greenland, P. J. F. Harris, W. Hayes, M. E. Mackay, S. J. Rowan, *Chem. Commun.* **2009**, *44*, 6717.
[40] L. Brunsveld, B. J. Folmer, E. W. Meijer, R. P. Sijbesma, *Chem. Rev.* **2001**, *101*, 4071.
[41] Y. Shi, M. Wang, C. Ma, Y. Wang, X. Li, G. Yu, *Nano Lett.* **2015**, *15*, 6276.
[42] C.-H. Li, J.-L. Zuo, *Adv. Mater.* **2020**, *32*, 1903762.
[43] C. Gu, M. Wang, K. Zhang, J. Li, Y.-L. Lu, Y. Cui, Y. Zhang, C.-S. Liu, *Adv. Mater.* **2023**, *35*, 2208392.
[44] S. Terryn, J. Brancart, D. Lefeber, G. Van Assche, B. Vanderborght, *Sci. Rob.* **2017**, *2*, eaan4268.
[45] S. Terryn, J. Brancart, E. Roels, R. Verhelle, A. Safaei, A. Cuvellier, B. Vanderborght, G. Van Assche, *Macromolecules* **2022**, *55*, 5497.
[46] E. F. Gomez, S. V. Wanasinghe, A. E. Flynn, O. J. Dodo, J. L. Sparks, L. A. Baldwin, C. E. Tabor, M. F. Durstock, D. Konkolewicz, C. J. Thrasher, *ACS Appl. Mater. Interfaces* **2021**, *13*, 28870.
[47] P. Froimowicz, H. Frey, K. Landfester, *Macromol. Rapid Commun.* **2011**, *32*, 468.
[48] E. Roels, S. Terryn, J. Brancart, R. Verhelle, G. Van Assche, B. Vanderborght, *Soft Rob.* **2020**, *7*, 711.
[49] H. Guo, Y. J. Tan, G. Chen, Z. Wang, G. J. Susanto, H. H. See, Z. Yang, Z. W. Lim, L. Yang, B. C. K. Tee, *Nat. Commun.* **2020**, *11*, 5747.
[50] R. B. Bird, *Appl. Mech. Rev.* **2002**, *55*, R1.
[51] Z. Zhang, X. Ni, H. Wu, M. Sun, G. Bao, H. Wu, S. Jiang, *Soft Rob.* **2022**, *9*, 57.
[52] C. Zhang, L. Zhao, R. Chen, R. Cao, Q. Zhao, C. Wang, Y. Hu, D. Wu, *Adv. Intell. Syst.* **2022**, *4*, 2200103.
[53] A. Cuvellier, R. Verhelle, J. Brancart, B. Vanderborght, G. Van Assche, H. Rahier, *Polym. Chem.* **2019**, *10*, 473.
[54] S. Terryn, J. Brancart, E. Roels, G. Van Assche, B. Vanderborght, *IEEE Rob. Autom. Mag.* **2020**, *27*, 44.
[55] D. B. Cardoso, E. Tavares de Andrade, R. A. A. Calderón, M. H. S. Rabelo, C. De Almeida Dias, I. Á. Lemos, *Coffee Sci.* **2018**, *13*, 498.
[56] V. Murashov, M. A. White, *J. Mater. Sci.* **2000**, *35*, 649.
[57] V. R. Tarnawski, T. Momose, W. Leong, G. Bovesecchi, P. Coppa, *Int. J. Thermophys.* **2009**, *30*, 949.
[58] X. Yang, C. Liang, T. Ma, Y. Guo, J. Kong, J. Gu, M. Chen, J. Zhu, *Adv. Compos. Hybrid Mater.* **2018**, *1*, 207.
[59] C. Wong, R. S. Bollampally, *J. Appl. Polym. Sci.* **1999**, *74*, 3396.
[60] X.-J. Wang, L.-Z. Zhang, L.-X. Pei, *J. Appl. Polym. Sci.* **2014**, *131*, 39550.